

# Anomalous enhancement of dilepton production as a precursor of color superconductivity

Toru Nishimura<sup>a,\*</sup>, Masakiyo Kitazawa<sup>a,b</sup>, Teiji Kunihiro<sup>c</sup>

<sup>a</sup>Department of Physics, Osaka University, Toyonaka, Osaka, 560-0043 Japan

<sup>b</sup>J-PARC Branch, KEK Theory Center, Institute of Particle and Nuclear Studies, KEK, 319-1106 Japan

<sup>c</sup>Yukawa Institute for Theoretical Physics, Kyoto University, Kyoto, 606-8502 Japan

## Abstract

We compute the modification of the photon self-energy due to dynamical diquark fluctuations developed near the critical temperature of the color superconductivity through the Aslamasov-Larkin, Maki-Thompson and density of states terms, which are responsible for the paraconductivity in metals at vanishing energy and momentum. It is shown that the rate has a significant enhancement at low invariant-mass region over a rather wide range of temperature in the normal phase. This enhancement is worth exploration in the relativistic heavy-ion collisions, which may thereby reveal the significance of the diquark fluctuations in dense quark matter.

*Keywords:* dilepton production rates, precursors of color superconductivity, diquark fluctuations, soft mode

## 1. Introduction

Revealing the rich phase structure and thereby developing a condensed matter physics of Quantum Chromodynamics (QCD) in the high density region is one of the main subjects in current nuclear physics [1, 2], and much endeavor has been being made both theoretically and experimentally. In the high density region, for instance, the first-order chiral transition line(s) with the QCD critical point(s) are expected to exist on the basis of theoretical works [3, 4, 5], and the experimental search for these phase transitions [6] is one of the main purposes of the beam-energy scan program in the relativistic heavy-ion collisions (HIC) at RHIC, HADES and NA61/SHINE; further studies to reveal the phase structure with higher statistics will be pursued in future experiments planned at GSI-FAIR, NICA-MPD and J-PARC-HI [7]. Such studies on the Earth will also provide us with invaluable information on the interior structure of compact stars [8, 9, 10].

An interesting feature of the dense quark matter in yet higher density region is the possible realization of the color superconductivity (CSC) induced by the condensation of diquark Cooper pairs [11]. Now that the future HIC experiments are designed so as to enable detailed analyses of the dense matter, it would be intriguing to explore the possible existence of the CSC phases in these experiments. The search for the CSC in the HIC, however, is quite a challenge because the temperatures  $T$  achieved in the HIC can become as high as 100 MeV at the highest baryon density [12], which may be much higher than the critical temperature  $T_c$  of the CSC, and hence an observation of the CSC phases can be unlikely in the HIC.

Nevertheless, the matter created in the HIC may be within the critical region above  $T_c$  where the diquark-pair fluctuations are significant, and thus *precursory phenomena* of the

CSC [13, 14, 15] do manifest themselves through appropriate observables by the HIC. In this respect, it is suggestive that fluctuations of Cooper pairs (preformed pairs) of electrons in metals are known to cause an anomalous enhancement of the electric conductivity above  $T_c$  of the superconductivity (SC) [16, 17]. Moreover, since the quark matter in the relevant density region is a strongly-coupled system [18, 14], the CSC can have a wider critical region where the precursory phenomena of the CSC are pronounced. In fact, it has been already shown [13, 14, 19, 15, 20, 21, 22] that the diquark fluctuations develop a well-defined collective mode, which is the soft mode of the CSC, and its collectivity and the softening nature affect various observables including the appearance of the “pseudo-gap” region [14] in a rather wide range of temperature.

In the present Letter, we investigate possible enhancement of the production rate of virtual photons due to the precursory diquark fluctuations, which is to be observed as the dilepton production rate (DPR) in the HIC. A desirable feature of the electromagnetic probes, needless to say, lies in the fact that the interactions of the probes with the medium are weak, and their properties are hardly modified from what they had when created, in contrast to hadronic signals.

Here we remark that the DPR in the CSC phases below  $T_c$  is known to show some unique behavior [23]. However, such a behavior becomes weaker when  $T$  goes higher and closer to  $T_c$  because they are caused by the finite diquark gap. On the other hand, the precursory phenomena to be investigated in the present Letter are most enhanced at  $T = T_c$ , which is an attractive feature in the HIC.

The medium modification of the DPR or the virtual photons is dictated by that of the photon self-energy [24, 25, 26]. The effects of the diquark fluctuations on the photon self-energy can be taken into account by the Aslamasov-Larkin, Maki-Thompson and density of states terms [15, 20, 22]. In the

\*Corresponding author

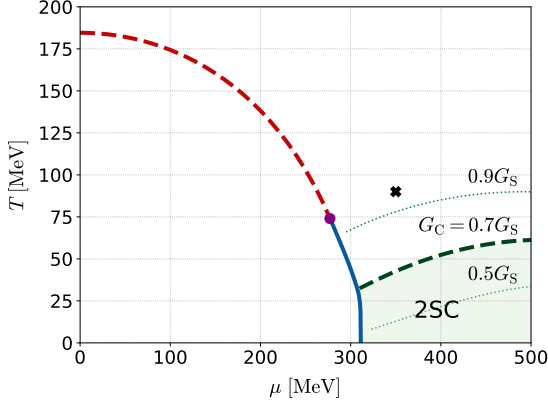


Figure 1: Phase diagram obtained in the massless 2-flavor NJL model Eq. (1). The bold lines show the transition lines at  $G_C = 0.7G_S$ . The solid and dashed lines represent the first- and second-order phase transitions. The  $T_c$  of the 2SC phase at  $G_C = 0.5G_S$  and  $0.9G_S$  are also shown by the thin-dotted lines.

case of the metallic SC, these terms at the vanishing energy-momentum limit are known to explain an anomalous enhancement of the electric conductivity above  $T_c$  [16, 17].

In the present Letter, we calculate these terms composed of diquark fluctuations near but above  $T_c$  of the CSC at nonzero energy and momentum. We show that the Ward-Takahashi (WT) identity is satisfied by summing up all of these terms. From the imaginary part of these terms we calculate a virtual photon emission from the diquark fluctuations that form a collective mode. It is found that the virtual photons emitted from the collective mode having a spectral support in the space-like region in turn have the spectral support in the time-like region. Our numerical results show that the DPR is significantly enhanced at low invariant-mass region  $M \lesssim 200$  MeV above  $T_c$  up to, say,  $T \approx 1.5T_c$ , reflecting the critical enhancement of the diquark fluctuations. We argue that an experimental measurement of dileptons and exploration of the possible enhancement of the DPR in that far low-mass region in the HIC is quite worthwhile to do because it would give an experimental evidence of strong diquark correlations as a precursor of the phase transition to CSC in dense quark matter.

## 2. Model and phase diagram

In this Letter, we consider the diquark fluctuations above  $T_c$  of the 2-flavor superconductor (2SC), which is one of the CSC phases that realizes at relatively low density [11]. We employ the 2-flavor NJL model [27, 28] as an effective model of QCD to describe the phase transition to 2SC;

$$\mathcal{L} = \bar{\psi}i\partial\psi + \mathcal{L}_S + \mathcal{L}_C, \quad (1)$$

$$\mathcal{L}_S = G_S[(\bar{\psi}\psi)^2 + (\bar{\psi}i\gamma_5\vec{\tau}\psi)^2], \quad (2)$$

$$\mathcal{L}_C = G_C(\bar{\psi}i\gamma_5\tau_2\lambda_A\psi^C)(\bar{\psi}^C i\gamma_5\tau_2\lambda_A\psi), \quad (3)$$

where  $\mathcal{L}_S$  and  $\mathcal{L}_C$  represent the quark-antiquark and quark-quark interactions, respectively, and  $\psi^C(x) = i\gamma_2\gamma_0\bar{\psi}^T(x)$ .  $\tau_2$  and  $\gamma_A$  ( $A = 2, 5, 7$ ) are the antisymmetric components of the Pauli and Gell-mann matrices for the flavor  $SU(2)_f$  and

$$\text{---} \Rightarrow \text{---} = G_C + \text{---} \text{---} \text{---} + \text{---} \text{---} \text{---} + \dots$$

Figure 2: Diagrammatic representation of the T-matrix Eq. (6) in the RPA.

color  $SU(3)_c$ , respectively. The scalar coupling constant  $G_S = 5.01\text{GeV}^{-2}$  and the three-momentum cutoff  $\Lambda = 650$  MeV are determined so as to reproduce the pion decay constant  $f_\pi = 93\text{MeV}$  and the chiral condensate  $\langle\bar{\psi}\psi\rangle = (-250\text{MeV})^3$  in vacuum [27]. The current quark mass is neglected for simplicity, while the diquark coupling  $G_C$  is treated as a free parameter. We employ a common quark chemical potential  $\mu$  for up and down quarks since the effect of isospin breaking is not large in the medium created in the HIC.

In Fig. 1, we show the phase diagram in the  $T$ - $\mu$  plane obtained in the mean-field approximation (MFA) with the mean fields  $\langle\bar{\psi}\psi\rangle$  and  $\langle\bar{\psi}^C\Gamma\psi\rangle$  with  $\Gamma = i\gamma_5\tau_2\lambda_A$ . The bold lines show the phase diagram at  $G_C = 0.7G_S$ , where the solid and dashed lines represent the first- and second-order phase transitions, respectively. The 2SC phase is realized in the dense region at relatively low temperatures. In the figure, the phase boundary of the 2SC for  $G_C = 0.5G_S$  and  $0.9G_S$  is also shown by the thin-dotted lines.

In MFA, the phase transition to 2SC is of second order as shown in Fig. 1. It is known that the transition becomes first order due to the effect of gauge fields (gluons) in asymptotically high density region [29, 30, 31, 32]. On the other hand, the fate of the transition at lower densities has not been settled down to the best of the authors' knowledge. In the present study we thus assume that the transition is second or weak first order having the formation of the soft mode discussed below.

## 3. The soft mode of 2SC

### 3.1. Propagator of diquark field

A characteristic feature of the second-order phase transition is that the fluctuation amplitude of the order parameter diverges at  $T = T_c$ . To see such a divergence at the  $T_c$  of the 2SC, let us consider the imaginary-time propagator of the diquark field  $\Delta(x) = \bar{\psi}^C(x)\Gamma\psi(x)$ ,

$$\mathcal{D}(k) = - \int_0^{1/T} d\tau \int d^3\mathbf{x} \langle T_\tau \Delta^\dagger(x)\Delta(0) \rangle e^{i\nu_l\tau} e^{-i\mathbf{k}\cdot\mathbf{x}}, \quad (4)$$

where  $k = (\mathbf{k}, i\nu_l)$  is the four momentum of the diquark field with  $\nu_l$  the Matsubara frequency for bosons,  $\tau$  is the imaginary time, and  $T_\tau$  denotes the imaginary-time ordering. In the random-phase approximation (RPA), Eq. (4) is given by  $\mathcal{D}(k) = Q(k)/(1 + G_C Q(k))$  with the one-loop quark-quark correlation function

$$Q(k) = -8 \int_p \text{Tr}[\mathcal{G}_0(k-p)\mathcal{G}_0(p)], \quad (5)$$

where  $\mathcal{G}_0(p) = 1/[(i\omega_m + \mu)\gamma_0 - \mathbf{p}\cdot\boldsymbol{\gamma}]$  is the free quark propagator with  $p = (\mathbf{p}, i\omega_m)$  and the Matsubara frequency for fermions  $\omega_m$ , Tr denotes the trace over the Dirac indices, and

$\int_p = T \sum_m \int d^3 p / (2\pi)^3$ . We also introduce the T-matrix to describe the diquark fluctuation

$$\tilde{\Xi}(k) = \frac{1}{G_C^{-1} + Q(k)} = G_C - G_C \mathcal{D}(k) G_C, \quad (6)$$

which is diagrammatically represented in Fig. 2.

The retarded Green functions  $D^R(\mathbf{k}, \omega)$ ,  $Q^R(\mathbf{k}, \omega)$  and  $\Xi^R(\mathbf{k}, \omega)$  corresponding to Eqs. (4)–(6), respectively, are obtained by the analytic continuation  $i\nu_l \rightarrow \omega + i\eta$ . The imaginary part of  $Q^R(\mathbf{k}, \omega)$  is calculated to be [15]

$$\begin{aligned} \text{Im}Q^R(\mathbf{k}, \omega) = & -\frac{2T}{\pi k} [(\omega + 2\mu)^2 - k^2] \\ & \times \left\{ \log \frac{\cosh(\omega + k)/4T}{\cosh(\omega - k)/4T} - \frac{\omega}{2T} \theta(k - |\omega + 2\mu|) \right\}. \end{aligned} \quad (7)$$

Its real part is then constructed using the Kramers-Kronig relation

$$\text{Re}Q^R(\mathbf{k}, \omega) = \frac{1}{\pi} P \int_{-2\Lambda-2\mu}^{2\Lambda-2\mu} d\omega' \frac{\text{Im}Q^R(\mathbf{k}, \omega')}{\omega' - \omega}, \quad (8)$$

where  $P$  denotes the principal value [15].

The retarded diquark propagator  $D^R(\mathbf{k}, \omega)$ , and hence the T-matrix  $\Xi^R(\mathbf{k}, \omega)$ , has a pole at  $\omega = |\mathbf{k}| = 0$  at  $T = T_c$ ;  $[D^R(\mathbf{0}, 0)]_{T=T_c}^{-1} = [\Xi^R(\mathbf{0}, 0)]_{T=T_c}^{-1} = 0$ . This fact, known as the Thouless criterion [33], is confirmed by comparing the denominator of  $D^R(\mathbf{k}, \omega)$  with the gap equation for the diquark field. The criterion shows that the diquark field has a massless collective mode at  $T = T_c$ . Furthermore, the pole of this collective mode moves continuously toward the origin in the complex energy plane as  $T$  is lowered to  $T_c$ , and hence the collective mode has a vanishing excitation energy toward  $T_c$ . This collective mode is called the *soft mode*. Because of the small excitation energy, they tend to be easily excited and affect various observables in the medium near  $T_c$  [14, 15].

Although we had recourse to the MFA and RPA, the appearance of a soft mode is a generic feature of the second-order phase transition [17], and even if the phase transition is of first order, the development of a collective mode with the softening nature prior to the critical point is still expected for weak first-order transitions. Therefore, the emergence of the soft mode in the diquark channel and the following discussions on its effects on observables should have a model-independent validity, at least qualitatively.

To detail the properties of the soft mode, it is convenient to introduce the dynamical structure factor  $S(\mathbf{k}, \omega)$  given by

$$S(\mathbf{k}, \omega) = -\frac{1}{\pi} \frac{1}{1 - e^{-\beta\omega}} \text{Im}D^R(\mathbf{k}, \omega). \quad (9)$$

Figure 3 shows a contour map of  $S(\mathbf{k}, \omega)$  at  $T = 1.05T_c$  for  $\mu = 350$  MeV and  $G_C = 0.7G_S$ . One sees that  $S(\mathbf{k}, \omega)$  has a clear spectral concentration with a peak around the origin in the  $\omega$ – $|\mathbf{k}|$  plane, which implies a development of the collective mode having a definite dispersion relation  $\omega = \omega(|\mathbf{k}|)$  with a small width [13, 15]. We also note that the spectral concentration is confined in the space-like region,  $\omega(|\mathbf{k}|) < |\mathbf{k}|$ . This feature will be picked up again later when we discuss the DPR that has a spectral support in the time-like region.

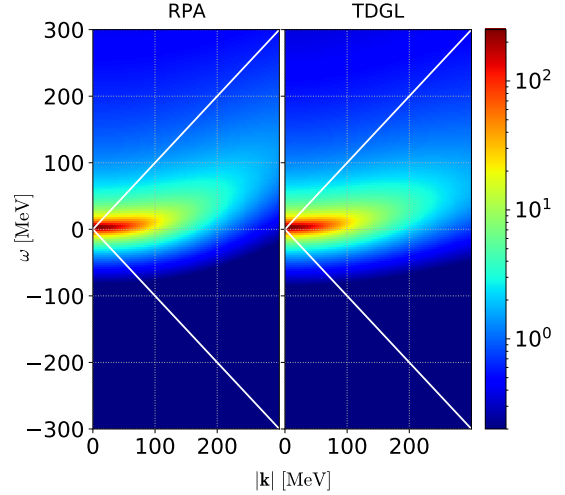


Figure 3: Contour plot of the dynamical structure factor  $S(\mathbf{k}, \omega)$  at  $T = 1.05T_c$  for  $\mu = 350$  MeV and  $G_C = 0.7G_S$ . The solid lines show the light cone. The left panel is the result of RPA obtained from Eqs. (7) and (8), while the right panel is the result in the TDGL approximation Eq. (10).

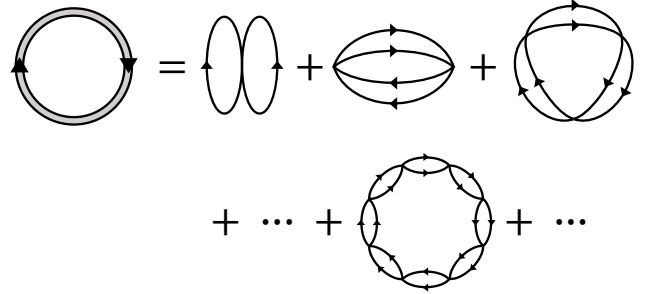


Figure 4: Contribution of the diquark fluctuations to the thermodynamic potential.

### 3.2. Time-dependent Ginzburg-Landau (TDGL) approximation

Since the diquark fluctuations near  $T_c$  have spectral concentration in the low energy region as we have seen above, we approximate the T-matrix  $\Xi^R(\mathbf{k}, \omega)$  in the small  $\omega$  region as

$$\Xi^R(\mathbf{k}, \omega) \simeq \frac{1}{c\omega + G_C^{-1} + Q^R(\mathbf{k}, 0)}, \quad (10)$$

with  $c = \partial Q^R(\mathbf{0}, \omega) / \partial \omega|_{\omega=0}$ . We refer Eq. (10) to as the time-dependent Ginzburg-Landau (TDGL) approximation, since Eq. (10) corresponds to the linearized TDGL approximation for the T-matrix [34] without the expansion along  $|\mathbf{k}|^2$ . In this study we do not expand  $[\Xi^R(\mathbf{k}, \omega)]^{-1}$  with respect to  $|\mathbf{k}|^2$  for a better description of the spectral strength extending along  $|\mathbf{k}|$  direction widely as in Fig. 3. An explicit calculation shows that  $c$  is a complex number, while  $G_C^{-1} + Q^R(\mathbf{k}, 0)$  is real.

In the right panel of Fig. 3, we show  $S(\mathbf{k}, \omega)$  obtained by the TDGL approximation. By comparing the result with the left panel, one sees that the TDGL approximation Eq. (10) reproduces the result obtained by the RPA quite well in a wide range in the  $\omega$ – $|\mathbf{k}|$  plane.

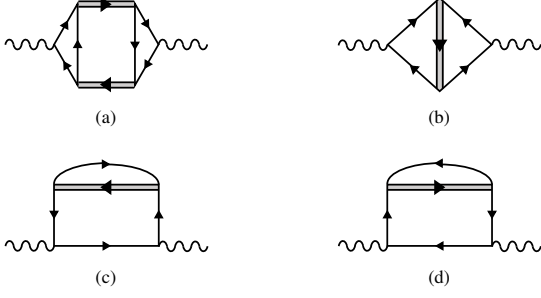


Figure 5: Diagrammatic representations of the Aslamasov-Larkin (a), Maki-Thompson (b) and density of states (c,d) terms in Eqs. (12)–(14). The double and wavy lines represent diquarks and photons, respectively.

#### 4. Photon self-energy and dilepton production rate

The DPR is given in terms of the retarded photon self-energy  $\Pi^{R\mu\nu}(\mathbf{k}, \omega)$  as [24, 25, 26],

$$\frac{d^4\Gamma(\mathbf{k}, \omega)}{d^4k} = -\frac{\alpha}{12\pi^4} \frac{1}{\omega^2 - |\mathbf{k}|^2} \frac{1}{e^{\beta\omega} - 1} g_{\mu\nu} \text{Im}\Pi^{R\mu\nu}(\mathbf{k}, \omega), \quad (11)$$

with the fine structure constant  $\alpha$ .

##### 4.1. Construction of the photon self-energy

We are now in a position to discuss the way how the effects of the diquark fluctuations are included in  $\Pi^{R\mu\nu}(\mathbf{k}, \omega)$ . For that, we start from the one-loop diagram of the diquark propagator shown in Fig. 4, which is the lowest-order contribution of the diquark fluctuations to the thermodynamic potential. The photon self-energy is then constructed by attaching electromagnetic vertices at two points of quark lines in Fig. 4. This construction guarantees the WT identity  $k_\nu \Pi^{R\mu\nu}(\mathbf{k}, \omega) = 0$ . This procedure leads to four types of diagrams shown in Fig. 5, which are called (a) Aslamasov-Larkin (AL) [35], (b) Maki-Thompson (MT) [36, 37] and (c,d) density of states (DOS) terms, respectively, in the theory of metallic SC [17]. The respective contributions to the photon self-energy are denoted by  $\tilde{\Pi}_{\text{AL}}^{\mu\nu}(k)$ ,  $\tilde{\Pi}_{\text{MT}}^{\mu\nu}(k)$  and  $\tilde{\Pi}_{\text{DOS}}^{\mu\nu}(k)$  in the imaginary-time formalism, which are expressed as

$$\tilde{\Pi}_{\text{AL}}^{\mu\nu}(k) = 3 \int_q \tilde{\Gamma}^\mu(q, q+k) \tilde{\Xi}(q+k) \tilde{\Gamma}^\nu(q+k, q) \tilde{\Xi}(q), \quad (12)$$

$$\tilde{\Pi}_{\text{MT}}^{\mu\nu}(k) = 3 \int_q \tilde{\Xi}(q) \mathcal{R}_{\text{MT}}^{\mu\nu}(q, k), \quad (13)$$

$$\tilde{\Pi}_{\text{DOS}}^{\mu\nu}(k) = 3 \int_q \tilde{\Xi}(q) \mathcal{R}_{\text{DOS}}^{\mu\nu}(q, k), \quad (14)$$

respectively, where  $q = (\mathbf{q}, i\nu_n)$  is the four momentum of a diquark field and the overall coefficients 3 come from three anti-symmetric channels of the diquark field. The vertex functions  $\tilde{\Gamma}^\mu(q, k)$ ,  $\mathcal{R}_{\text{MT}}^{\mu\nu}(q, k)$  and  $\mathcal{R}_{\text{DOS}}^{\mu\nu}(q, k)$  in Eqs. (12)–(14) are given

by

$$\tilde{\Gamma}^\mu(q, q+k) = 8(e_u + e_d) \int_p \text{Tr}[\mathcal{G}_0(p) \gamma^\mu \mathcal{G}_0(p+k) \mathcal{G}_0(q-p)], \quad (15)$$

$$\mathcal{R}_{\text{MT}}^{\mu\nu}(q, k) = 16e_u e_d \times \int_p \text{Tr}[\mathcal{G}_0(p) \gamma^\mu \mathcal{G}_0(p+k) \mathcal{G}_0(q-p-k) \gamma^\nu \mathcal{G}_0(q-p)], \quad (16)$$

$$\mathcal{R}_{\text{DOS}}^{\mu\nu}(q, k) = 8(e_u^2 + e_d^2) \times \int_p \left\{ \text{Tr}[\mathcal{G}_0(p) \gamma^\mu \mathcal{G}_0(p+k) \gamma^\nu \mathcal{G}_0(p) \mathcal{G}_0(q-p)] + \text{Tr}[\mathcal{G}_0(p) \gamma^\mu \mathcal{G}_0(p-k) \gamma^\nu \mathcal{G}_0(p) \mathcal{G}_0(q-p)] \right\}. \quad (17)$$

where  $e_u = 2|e|/3$  and  $e_d = -|e|/3$  are the electric charges of up and down quarks, respectively, with the elementary charge  $e$ .

The total photon self-energy in imaginary time is given by

$$\tilde{\Pi}^{\mu\nu}(k) = \tilde{\Pi}_{\text{free}}^{\mu\nu}(k) + \tilde{\Pi}_{\text{fluc}}^{\mu\nu}(k), \quad (18)$$

$$\tilde{\Pi}_{\text{fluc}}^{\mu\nu}(k) = \tilde{\Pi}_{\text{AL}}^{\mu\nu}(k) + \tilde{\Pi}_{\text{MT}}^{\mu\nu}(k) + \tilde{\Pi}_{\text{DOS}}^{\mu\nu}(k), \quad (19)$$

where  $\tilde{\Pi}_{\text{fluc}}^{\mu\nu}(k)$  denotes the modification of the self-energy due to the diquark fluctuations and  $\tilde{\Pi}_{\text{free}}^{\mu\nu}(k)$  is that of the free quark system [38, 39].

##### 4.2. Vertices

The vertices (15)–(17) satisfy the WT identities

$$k_\mu \tilde{\Gamma}^\mu(q, q+k) = e_\Delta (\mathcal{Q}(q+k) - \mathcal{Q}(q)) = e_\Delta \left( \frac{1}{\tilde{\Xi}(q+k)} - \frac{1}{\tilde{\Xi}(q)} \right), \quad (20)$$

$$k_\mu \mathcal{R}^{\mu\nu}(q, k) = e_\Delta (\Gamma^\nu(q-k, q) - \Gamma^\nu(q, q+k)), \quad (21)$$

with  $\mathcal{R}^{\mu\nu}(q, k) = \mathcal{R}_{\text{MT}}^{\mu\nu}(q, k) + \mathcal{R}_{\text{DOS}}^{\mu\nu}(q, k)$  and  $e_\Delta = e_u + e_d$  being the electric charge of diquarks. Using Eqs. (20), (21) and  $\tilde{\Gamma}^\nu(q, q+k) = \tilde{\Gamma}^\nu(q+k, q)$ , the WT identity of the photon self-energy  $k_\nu \tilde{\Pi}_{\text{fluc}}^{\mu\nu}(k) = 0$  is shown explicitly as

$$\begin{aligned} k_\mu \tilde{\Pi}_{\text{fluc}}^{\mu\nu}(k) &= k_\mu \tilde{\Pi}_{\text{AL}}^{\mu\nu}(k) + k_\mu \{ \tilde{\Pi}_{\text{MT}}^{\mu\nu}(k) + \tilde{\Pi}_{\text{DOS}}^{\mu\nu}(k) \} \\ &= -3e_\Delta \int_q [\tilde{\Xi}(q+k) - \tilde{\Xi}(q)] \tilde{\Gamma}^\nu(q, q+k) \\ &\quad + 3e_\Delta \int_q \tilde{\Xi}(q) [\tilde{\Gamma}^\nu(q-k, q) - \tilde{\Gamma}^\nu(q, q+k)] \\ &= 0. \end{aligned} \quad (22)$$

Since we adopt the TDGL approximation for  $\Xi^R(\mathbf{k}, \omega)$ , the vertices  $\tilde{\Gamma}^\mu(q, q+k)$  and  $\mathcal{R}^{\mu\nu}(q, k)$  have to be approximated to satisfy Eqs. (20) and (21) within this approximation. From Eq. (10) one finds

$$\begin{aligned} [\tilde{\Xi}(q+k)]^{-1} - [\tilde{\Xi}(q)]^{-1} &\simeq c_0 i\nu_n + \mathcal{Q}(\mathbf{q} + \mathbf{k}, 0) - \mathcal{Q}(\mathbf{q}, 0) \\ &= c_0 i\nu_n + \frac{\mathcal{Q}(\mathbf{q} + \mathbf{k}, 0) - \mathcal{Q}(\mathbf{q}, 0)}{|\mathbf{q} + \mathbf{k}|^2 - |\mathbf{q}|^2} (|\mathbf{q} + \mathbf{k}|^2 - |\mathbf{q}|^2) \\ &= c_0 i\nu_n + \mathcal{Q}_{(1)}(\mathbf{q} + \mathbf{k}, \mathbf{q}) (2\mathbf{q} + \mathbf{k}) \cdot \mathbf{k}, \end{aligned} \quad (23)$$



where  $Q_{(1)}(\mathbf{q}_1, \mathbf{q}_2) = (Q(\mathbf{q}_1, 0) - Q(\mathbf{q}_2, 0))/(|\mathbf{q}_1|^2 - |\mathbf{q}_2|^2)$  is finite in the limit  $|\mathbf{q}_1 - \mathbf{q}_2| \rightarrow 0$  because  $Q(\mathbf{q}, \omega)$  is a function of  $|\mathbf{q}|^2$ . Substituting Eq. (23) into Eq. (20) and requiring the analyticity of  $\tilde{\Gamma}^\mu(q, q+k)$  at  $\omega = |\mathbf{k}| = 0$  one finds that  $\tilde{\Gamma}^0(q, q+k) = e_{\Delta} c_0$  and

$$\tilde{\Gamma}^i(q, q+k) = -e_{\Delta} Q_{(1)}(\mathbf{q} + \mathbf{k}, \mathbf{q})(2q+k)^i, \quad (24)$$

are choices that satisfy Eq. (20), where  $i = 1, 2, 3$ . One can also obtain forms of  $\mathcal{R}^{\mu\nu}(q, k)$  satisfying Eq. (21) with Eq. (24) in a similar manner, which, however, are not shown explicitly since they turn out unnecessary in this study as discussed below. These vertices with Eq. (10) satisfy the WT identity of  $\tilde{\Pi}^{\mu\nu}(k)$ . It should be warned, however, that the uniqueness of the choice of Eq. (24) holds only in the lowest order of  $\omega$  and  $|\mathbf{k}|^2$ , and hence the non-uniqueness may affect the final result in the high energy region.

### 4.3. Dilepton production rate

In the above construction of  $\tilde{\Gamma}^\mu(q, q+k)$  and  $\mathcal{R}^{\mu\nu}(q, k)$ , the spatial components of these vertices are real. This fact greatly simplifies the analytic continuation from  $\tilde{\Pi}_{\text{fluc}}^{ij}(k)$  to  $\Pi_{\text{fluc}}^{Rij}(\mathbf{k}, \omega)$ . From the reality of  $\mathcal{R}^{ij}(q, k)$  it is also shown that  $\text{Im}[\Pi_{\text{MT}}^{Rij}(\mathbf{k}, \omega) + \Pi_{\text{DOS}}^{Rij}(\mathbf{k}, \omega)] = 0$  [17], which means that the spatial components  $\text{Im}\Pi_{\text{fluc}}^{Rij}(\mathbf{k}, \omega)$  only come from  $\Pi_{\text{AL}}^{Rij}(\mathbf{k}, \omega)$ , while the temporal component  $\text{Im}\Pi_{\text{fluc}}^{R00}(\mathbf{k}, \omega)$  is given by the sum of AL, MT and DOS terms. The temporal component, however, is obtained from the spatial ones using the WT identity

$$\tilde{\Pi}^{00}(k) = \frac{\mathbf{k}^2}{(iv_l)^2} \tilde{\Pi}^{11}(k), \quad (25)$$

with  $k = (iv_l, |\mathbf{k}|, 0, 0)$ . One then finds that  $g_{\mu\nu} \tilde{\Pi}_{\text{fluc}}^{\mu\nu}(k)$  in Eq. (11) is obtained only from  $\Pi_{\text{AL}}^{Rij}(\mathbf{k}, \omega)$  as

$$\begin{aligned} g_{\mu\nu} \tilde{\Pi}_{\text{fluc}}^{\mu\nu}(k) &= \frac{\mathbf{k}^2}{(iv_l)^2} \tilde{\Pi}_{\text{AL}}^{11}(k) - \sum_{i=1}^3 \tilde{\Pi}_{\text{AL}}^{ii}(k) \\ &= 3 \int \frac{d^3 \mathbf{q}}{(2\pi)^3} \left[ \frac{\mathbf{k}^2}{(iv_l)^2} (\tilde{\Gamma}^1(q, q+k))^2 - \sum_i (\tilde{\Gamma}^i(q, q+k))^2 \right] \\ &\quad \times \oint_C \frac{dq_0}{2\pi i} \frac{\coth \frac{q_0}{2T}}{2} \tilde{\Xi}(\mathbf{q} + \mathbf{k}, q_0 + iv_l) \tilde{\Xi}(\mathbf{q}, q_0) \quad (26) \\ &= 3 \int \frac{d^3 \mathbf{q}}{(2\pi)^3} \left[ \frac{\mathbf{k}^2}{(iv_l)^2} (\tilde{\Gamma}^1(q, q+k))^2 - \sum_i (\tilde{\Gamma}^i(q, q+k))^2 \right] \\ &\quad \times \left\{ P \int \frac{d\omega'}{2\pi i} \frac{\coth \frac{\omega'}{2T}}{2} \Xi^R(\mathbf{q} + \mathbf{k}, \omega' + iv_l) \Xi^R(\mathbf{q}, \omega') \right. \\ &\quad - P \int \frac{d\omega'}{2\pi i} \frac{\coth \frac{\omega'}{2T}}{2} \Xi^R(\mathbf{q} + \mathbf{k}, \omega' + iv_l) \Xi^A(\mathbf{q}, \omega') \\ &\quad + P \int \frac{d\omega'}{2\pi i} \frac{\coth \frac{\omega'}{2T}}{2} \Xi^R(\mathbf{q} + \mathbf{k}, \omega') \Xi^A(\mathbf{q}, \omega' - iv_l) \\ &\quad \left. - P \int \frac{d\omega'}{2\pi i} \frac{\coth \frac{\omega'}{2T}}{2} \Xi^A(\mathbf{q} + \mathbf{k}, \omega') \Xi^A(\mathbf{q}, \omega' - iv_l) \right\}, \quad (27) \end{aligned}$$

where the contour  $C$  in Eq. (26) surrounds the poles of  $\coth(q_0/2T)$  and  $\Xi^A(\mathbf{k}, \omega) = \tilde{\Xi}(k)|_{iv_l \rightarrow \omega - i\eta}$  is the advanced T-matrix. The far right-hand side Eq. (27) is obtained after deforming the contour  $C$  avoiding the cut in  $\tilde{\Xi}(q)$  on the real axis [17]. By taking the analytic continuation  $iv_l \rightarrow \omega + i\eta$  and using  $\Xi^A(\mathbf{k}, \omega) = [\Xi^R(\mathbf{k}, \omega)]^*$ , we obtain

$$\begin{aligned} g_{\mu\nu} \text{Im}\Pi_{\text{fluc}}^{R\mu\nu}(\mathbf{k}, \omega) &= 3e_{\Delta}^2 \int_{-2\Lambda-2\mu}^{2\Lambda-2\mu} \frac{d\omega'}{2\pi} \int \frac{d^3 \mathbf{q}}{(2\pi)^3} \coth \frac{\omega'}{2T} \\ &\quad \times (Q_{(1)}(\mathbf{q} + \mathbf{k}, \mathbf{q}))^2 \left[ \left( \frac{(\mathbf{q} + \mathbf{k})^2 - \mathbf{q}^2}{\omega} \right)^2 - (2\mathbf{q} + \mathbf{k})^2 \right] \\ &\quad \times \text{Im}\Xi^R(\mathbf{q} + \mathbf{k}, \omega') \{ \text{Im}\Xi^R(\mathbf{q}, \omega' + \omega) - \text{Im}\Xi^R(\mathbf{q}, \omega' - \omega) \}. \quad (28) \end{aligned}$$

To deal with the momentum integral in Eq. (28), we introduce the ultraviolet cutoff with the same procedure as in Ref. [15]. The DPR is obtained by substituting this result into Eq. (11).

## 5. Numerical results

In Fig. 6, we show the numerical results of the production rate  $d^4\Gamma/d^4k$  per unit energy and momentum at  $\mathbf{k} = \mathbf{0}$  calculated with use of the photon self-energy Eq. (18) and Eq. (28) for various values of  $T$  and  $\mu$  at  $G_C = 0.7G_S$ . The thick lines show the contribution of diquark fluctuations obtained from  $\Pi_{\text{fluc}}^{R\mu\nu}(\mathbf{k}, \omega)$ , while the thin lines are the results for the free quark gas. The total rate is given by the sum of these two contributions. The figure shows that the production rate is enhanced so much by the diquark fluctuations that it greatly exceeds that of the free quarks in the low energy region  $\omega \lesssim 300$  MeV. The enhancement is more pronounced as  $T$  is lowered toward  $T_c$ , while the enhancement at  $\omega \simeq 200$  MeV is observed up to  $T \simeq 1.5T_c$ . The figure also shows that the contribution of diquark fluctuations is more enhanced as  $\mu$  becomes larger. This behavior is understood as the effect of the larger Fermi surface for larger  $\mu$ .

It is found worth scrutinizing the underlying mechanism of the low-energy enhancement of the production mechanism of virtual photons. Although it is rather natural that  $d^4\Gamma/d^4k$  is enhanced in the low energy region since the virtual photons are emitted from the soft collective modes, their pronounced effects on the production of virtual photons in the *time-like* region deserves an elucidation since the soft mode has a dominant strength in the *space-like* region as shown in Fig. 3. In our formalism, the virtual photons are dominantly emitted through the process obtained by cutting Fig. 5 (a), i.e. the scattering of diquarks shown in the left panel of Fig. 7. In this process, energy-momentum of the virtual photon  $k = (\mathbf{k}, \omega)$  can be time-like,  $\omega > |\mathbf{k}|$ , since the absolute value of the momentum  $\mathbf{k} = \mathbf{q}_1 - \mathbf{q}_2$  can be taken arbitrarily small keeping  $\omega = \omega_1 - \omega_2$  finite. This kinematics is contrasted to the scattering of massless quarks shown in the right panel of Fig. 7, in which the produced virtual photon is always in the space-like region  $\omega < |\mathbf{k}|$ . However,  $\omega = \omega_1 - \omega_2$  of a virtual photon is restricted to small values due to the small energies  $\omega_1$  and  $\omega_2$  of diquarks. The sharp peak of  $d^4\Gamma/d^4k$  in Fig. 6 is understood in this way.

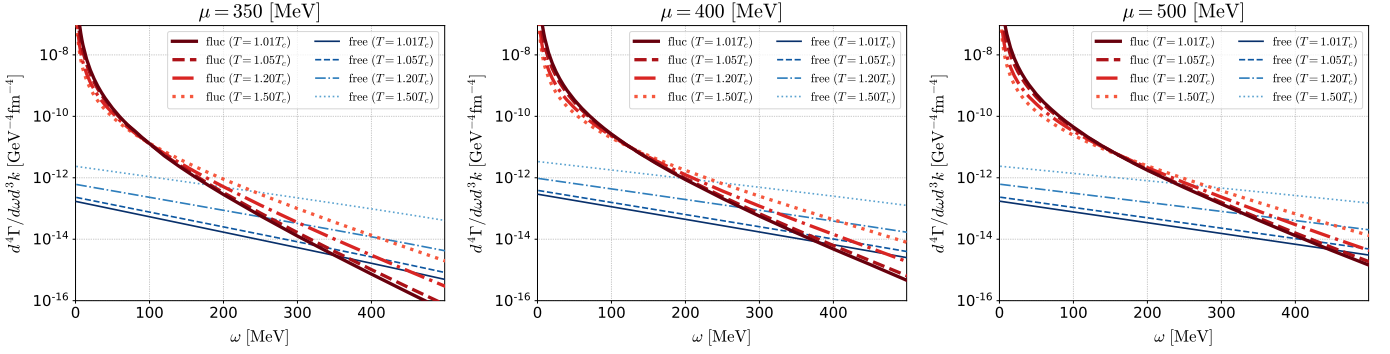


Figure 6: Dilepton production rates per unit energy and momentum  $d^4\Gamma/d\omega d^3k$  at  $k = 0$  for several values of  $T/T_c$  with  $\mu = 350$  MeV (left), 400 MeV (middle) and 500 MeV (right) and  $G_C = 0.7G_S$ . The thick-red (thin-blue) lines show the contribution of  $\bar{\Pi}_{\text{fluc}}^{\mu\nu}(k)$  ( $\bar{\Pi}_{\text{free}}^{\mu\nu}(k)$ ).

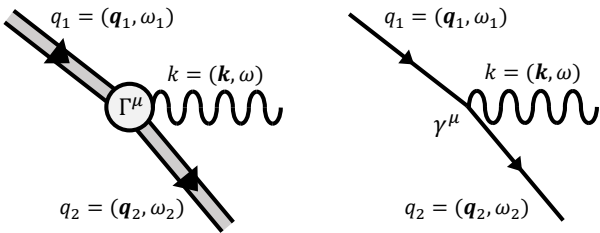


Figure 7: Diagrams representing the processes of a virtual photon production.

To have more detailed properties of the enhancement of DPR, we show in the far left panel of Fig. 8 a three-dimensional plot of DPR in the  $\omega$ - $|k|$  plane for several values of  $T$  at  $\mu = 350$  MeV and  $G_C = 0.7G_S$ . We see that the DPR is enhanced strongly around the origin in the  $\omega$ - $|k|$  plane, and the larger  $\omega$  and/or  $|k|$ , the smaller the DPR. This behavior is in accordance with the mechanism explained above.

In the HIC experiments, the dilepton production rate is usually measured as a function of the invariant mass,  $M$ ,

$$\frac{d\Gamma}{dM^2} = \int d^3k \frac{1}{2\omega} \frac{d^4\Gamma}{d^4k} \Big|_{\omega=\sqrt{k^2+M^2}}. \quad (29)$$

In the middle panel of Fig. 8, we show Eq. (29) for several values of  $T/T_c$  at  $G_C = 0.7G_S$  and  $\mu = 350$  MeV. One sees that the enhancement due to diquark fluctuations is observed in the low invariant-mass region  $M < (150 - 200)$  MeV up to  $T \simeq 1.5T_c$ . The little  $T$  dependence of DPR seen in the far low region of  $M$  may be understood as a result of an accidental cancellation between the enhanced spectral function due to the soft mode and the kinematical thermal effect: The sharp enhancement of the former at low energy-momentum near  $T_c$  decreases while the creation probability due to the thermal effect increases as  $T$  goes high. The contribution of the diquark fluctuations is relatively suppressed for higher  $T$  as the contribution of free quarks becomes larger.

Finally, shown in the right panel of Fig. 8 is  $d\Gamma/dM^2$  at fixed  $(T, \mu) = (90, 350)$  MeV (the cross symbol in Fig. 1) for several values of  $G_C$ . The panel shows that the production rate is more enhanced for larger  $G_C$  and  $T_c$ . For  $G_C = 0.9G_S$  ( $T_c \simeq 78$  MeV), the production rate from the diquark fluctuations exceeds those of the free quarks for  $M \lesssim 100$  MeV.

## 6. Discussions

In this Letter, we have investigated the effect of diquark fluctuations on the DPR near but above the critical temperature of the 2SC. The contribution of the diquark fluctuations were taken into account through the AL, MT and DOS terms in the photon self-energy. We have found that the dilepton production rate is strongly enhanced in comparison with the free-quark gases in the low energy and low invariant-mass regions near  $T_c$  up to  $T \simeq 1.5T_c$  reflecting the formation of the diquark soft mode associated with the phase transition to 2SC.

We would say that it should be rewarding to try to make an experimental measurement of dileptons in that far low-mass region and examine the possible enhancement of the DPR in the HIC; if the enhancement is confirmed, it may possibly give an experimental evidence of strong diquark correlations, which lead to the phase transition to CSC in dense quark matter. Moreover, it is to be noted that the DPR with vanishing energy/momentum is directly related to the electric conductivity, as is evident from the fact that the AL, MT and DOS terms in condensed matter physics are responsible for the anomalous enhancement of the electric conductivity (paraconductivity) in metals above  $T_c$  but in the close vicinity of the superconducting phase.

There are, however, many issues to be resolved for making the measurements meaningful, in the sense that it can help in revealing the significance of the diquark fluctuations prior to the phase transition to the 2SC in the dense matter. Since observed yield of the dilepton production in the HIC is a superposition of those with various origins in the space-time history, we need to ‘disentangle’ the observed total yield into those with the respective origins. For that, it is necessary to quantitatively estimate the residence time around the phase boundary of the CSC, say, with resort to dynamical models [40]. Even when some enhancement of the DPR in the low  $M$  region is identified, it is to be noted that it may have come from a different mechanism due to medium effects [41, 42, 43]. A comparison of our results with these effects constitutes future projects.

The experimental measurement of the DPR in the relevant low invariant-mass region  $M \lesssim 200$  MeV is not an easy task because di-electrons, which are, among dileptons, only available

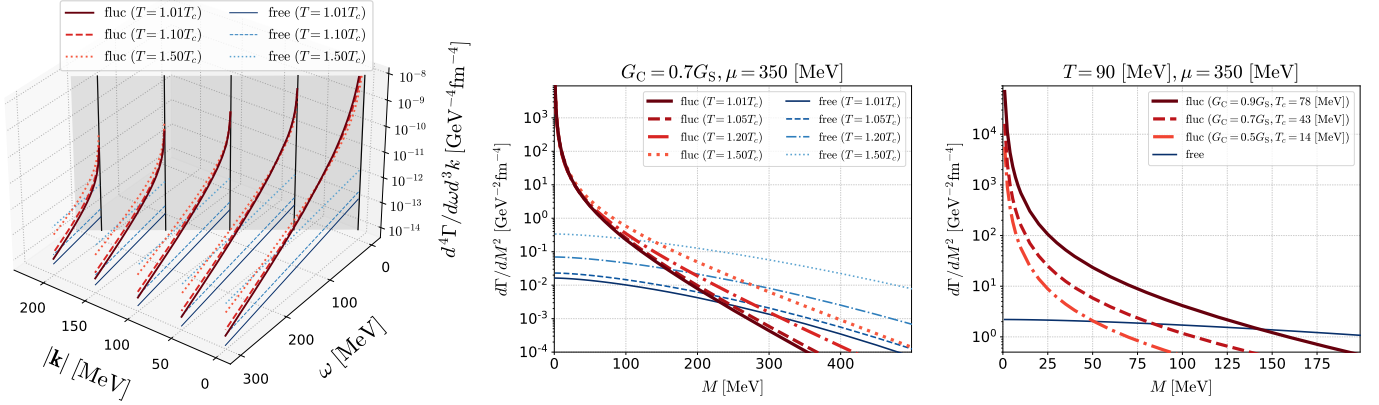


Figure 8: **Left:** Dilepton production rates  $d^4\Gamma/d\omega d^3k$  as a function of  $\omega$  and  $|k|$  for  $\mu = 350$  MeV and  $T = 1.01 T_c$ ,  $1.1 T_c$  and  $1.5 T_c$  at  $G_C = 0.7G_S$ . The gray surface shows the light-cone. **Middle:** The invariant-mass spectrum  $d\Gamma/dM^2$  for several values of  $T/T_c$  at  $G_C = 0.7G_S$  and  $\mu = 350$  MeV. **Right:** The invariant-mass spectrum  $d\Gamma/dM^2$  at  $(T, \mu) = (90, 350)$  MeV for  $G_C = 0.9G_S$  (solid),  $0.7G_S$  (dashed) and  $0.5G_S$  (dash-dotted).

in this energy range, are severely contaminated by the Dalitz decays, and high-precision measurements both of  $d\Gamma/dM^2$  and hadron spectrum are necessary to extract interesting medium effects. Despite these challenging requirements, it is encouraging that the future HIC programs in GSI-FAIR, NICA-MPD and J-PARC-HI are designed to carry out high-precision experiments [7], and also that new technical developments are vigorously being made [44].

Finally, we remark that such an effort to reveal the significance of the enhanced diquark correlations in the hot and dense matter should also give some clue to the modern development of hadron physics where possible diquark correlations in hadron structures are one of the hot topics [45].

## Acknowledgements

The authors thank Naoki Yamamoto for his critical comments. T. N. thanks JST SPRING (Grant No. JPMJSP2138) and Multidisciplinary PhD Program for Pioneering Quantum Beam Application. This work was supported by JSPS KAKENHI (Grants No. JP19K03872, No. JP90250977, and No. JP10323263).

## References

- [1] K. Fukushima, T. Hatsuda, The phase diagram of dense QCD, Rept. Prog. Phys. 74 (2011) 014001. [arXiv:1005.4814](#), [doi:10.1088/0034-4885/74/1/014001](#).
- [2] K. Fukushima, C. Sasaki, The phase diagram of nuclear and quark matter at high baryon density, Prog. Part. Nucl. Phys. 72 (2013) 99–154. [arXiv:1301.6377](#), [doi:10.1016/j.pnpnp.2013.05.003](#).
- [3] M. Asakawa, K. Yazaki, Chiral Restoration at Finite Density and Temperature, Nucl. Phys. A 504 (1989) 668–684. [doi:10.1016/0375-9474\(89\)90002-X](#).
- [4] A. Barducci, R. Casalbuoni, S. De Curtis, R. Gatto, G. Pettini, Chiral Symmetry Breaking in QCD at Finite Temperature and Density, Phys. Lett. B 231 (1989) 463–470. [doi:10.1016/0370-2693\(89\)90695-3](#).
- [5] M. Kitazawa, T. Koide, T. Kunihiro, Y. Nemoto, Chiral and color superconducting phase transitions with vector interaction in a simple model, Prog. Theor. Phys. 108 (5) (2002) 929–951, [Erratum: Prog.Theor.Phys. 110, 185–186 (2003)]. [arXiv:hep-ph/0207255](#), [doi:10.1143/PTP.108.929](#).

- [6] M. A. Stephanov, K. Rajagopal, E. V. Shuryak, Event-by-event fluctuations in heavy ion collisions and the QCD critical point, Phys. Rev. D 60 (1999) 114028. [arXiv:hep-ph/9903292](#), [doi:10.1103/PhysRevD.60.114028](#).
- [7] T. Galatyuk, Future facilities for high  $\mu_B$  physics, Nucl. Phys. A 982 (2019) 163–169. [doi:10.1016/j.nuclphysa.2018.11.025](#).
- [8] T. Kojo, D. Hou, J. Okafor, H. Togashi, Phenomenological QCD equations of state for neutron star dynamics: Nuclear-2SC continuity and evolving effective couplings, Phys. Rev. D 104 (6) (2021) 063036. [arXiv:2012.01650](#), [doi:10.1103/PhysRevD.104.063036](#).
- [9] M. Cierniak, D. Blaschke, Hybrid neutron stars in the mass-radius diagram, Astron. Nachr. 342 (5) (2021) 819–825. [arXiv:2106.06986](#), [doi:10.1002/asna.202114000](#).
- [10] T. Kojo, G. Baym, T. Hatsuda, QHC21 equation of state of neutron star matter - in light of 2021 NICER data (11 2021). [arXiv:2111.11919](#).
- [11] M. G. Alford, A. Schmitt, K. Rajagopal, T. Schäfer, Color superconductivity in dense quark matter, Rev. Mod. Phys. 80 (2008) 1455–1515. [arXiv:0709.4635](#), [doi:10.1103/RevModPhys.80.1455](#).
- [12] A. Ohnishi, Approaches to QCD phase diagram; effective models, strong-coupling lattice QCD, and compact stars, J. Phys. Conf. Ser. 668 (1) (2016) 012004. [arXiv:1512.08468](#), [doi:10.1088/1742-6596/668/1/012004](#).
- [13] M. Kitazawa, T. Koide, T. Kunihiro, Y. Nemoto, Precursor of color superconductivity in hot quark matter, Phys. Rev. D 65 (2002) 091504. [arXiv:nucl-th/0111022](#), [doi:10.1103/PhysRevD.65.091504](#).
- [14] M. Kitazawa, T. Koide, T. Kunihiro, Y. Nemoto, Pseudogap of color superconductivity in heated quark matter, Phys. Rev. D 70 (2004) 056003. [arXiv:hep-ph/0309026](#), [doi:10.1103/PhysRevD.70.056003](#).
- [15] M. Kitazawa, T. Koide, T. Kunihiro, Y. Nemoto, Pre-critical phenomena of two-flavor color superconductivity in heated quark matter: Diquark-pair fluctuations and non-Fermi liquid behavior, Prog. Theor. Phys. 114 (2005) 117–155. [arXiv:hep-ph/0502035](#), [doi:10.1143/PTP.114.117](#).
- [16] W. Skocpol, M. Tinkham, Fluctuations near superconducting phase transitions, Reports on Progress in Physics 38 (9) (1975) 1049.
- [17] A. Larkin, A. Varlamov, Fluctuation phenomena in superconductors, in: Superconductivity, Springer, 2008, pp. 369–458.
- [18] H. Abuki, T. Hatsuda, K. Itakura, Structural change of Cooper pairs and momentum dependent gap in color superconductivity, Phys. Rev. D 65 (2002) 074014. [arXiv:hep-ph/0109013](#), [doi:10.1103/PhysRevD.65.074014](#).
- [19] D. N. Voskresensky, Fluctuations of the color superconducting order parameter in heated and dense quark matter (6 2003). [arXiv:nucl-th/0306077](#).
- [20] T. Kunihiro, M. Kitazawa, Y. Nemoto, How do diquark fluctuations and chiral soft modes affect di-lepton production in the deconfined phase?, PoS CPOD07 (2007) 041. [arXiv:0711.4429](#), [doi:10.22323/1.047.0041](#).

- [21] B. O. Kerbikov, M. A. Andreichikov, Electrical Conductivity of Dense Quark Matter with Fluctuations and Magnetic Field Included, *Phys. Rev. D* 91 (7) (2015) 074010. [arXiv:1410.3413](#), [doi:10.1103/PhysRevD.91.074010](#).
- [22] B. O. Kerbikov, Precritical soft photon emission from quark matter, *Phys. Rev. D* 102 (9) (2020) 096022. [arXiv:2001.11766](#), [doi:10.1103/PhysRevD.102.096022](#).
- [23] P. Jaikumar, R. Rapp, I. Zahed, Photon and dilepton emission rates from high density quark matter, *Phys. Rev. C* 65 (2002) 055205. [arXiv:hep-ph/0112308](#), [doi:10.1103/PhysRevC.65.055205](#).
- [24] L. D. McLerran, T. Toimela, Photon and Dilepton Emission from the Quark - Gluon Plasma: Some General Considerations, *Phys. Rev. D* 31 (1985) 545. [doi:10.1103/PhysRevD.31.545](#).
- [25] H. A. Weldon, Reformulation of finite temperature dilepton production, *Phys. Rev. D* 42 (1990) 2384–2387. [doi:10.1103/PhysRevD.42.2384](#).
- [26] J. I. Kapusta, P. Lichard, D. Seibert, High-energy photons from quark - gluon plasma versus hot hadronic gas, *Phys. Rev. D* 44 (1991) 2774–2788, [Erratum: *Phys.Rev.D* 47, 4171 (1993)]. [doi:10.1103/PhysRevD.47.4171](#).
- [27] T. Hatsuda, T. Kunihiro, QCD phenomenology based on a chiral effective Lagrangian, *Phys. Rept.* 247 (1994) 221–367. [arXiv:hep-ph/9401310](#), [doi:10.1016/0370-1573\(94\)90022-1](#).
- [28] M. Buballa, NJL model analysis of quark matter at large density, *Phys. Rept.* 407 (2005) 205–376. [arXiv:hep-ph/0402234](#), [doi:10.1016/j.physrep.2004.11.004](#).
- [29] T. Matsuura, K. Iida, T. Hatsuda, G. Baym, Thermal fluctuations of gauge fields and first order phase transitions in color superconductivity, *Phys. Rev. D* 69 (2004) 074012. [arXiv:hep-ph/0312042](#), [doi:10.1103/PhysRevD.69.074012](#).
- [30] I. Giannakis, D.-f. Hou, H.-c. Ren, D. H. Rischke, Gauge field fluctuations and first-order phase transition in color superconductivity, *Phys. Rev. Lett.* 93 (2004) 232301. [arXiv:hep-ph/0406031](#), [doi:10.1103/PhysRevLett.93.232301](#).
- [31] J. L. Noronha, H.-c. Ren, I. Giannakis, D. Hou, D. H. Rischke, Absence of the London limit for the first-order phase transition to a color superconductor, *Phys. Rev. D* 73 (2006) 094009. [arXiv:hep-ph/0602218](#), [doi:10.1103/PhysRevD.73.094009](#).
- [32] G. Fejős, N. Yamamoto, Functional renormalization group approach to color superconducting phase transition, *JHEP* 12 (2019) 069. [arXiv:1908.03535](#), [doi:10.1007/JHEP12\(2019\)069](#).
- [33] D. J. Thouless, Perturbation theory in statistical mechanics and the theory of superconductivity, *Annals of Physics* 10 (4) (1960) 553–588.
- [34] M. Cyrot, Ginzburg-landau theory for superconductors, *Reports on Progress in Physics* 36 (2) (1973) 103.
- [35] L. Aslamazov, A. Larkin, Soviet solid state 10, 875 (1968), *Phys. Lett. A* 26 (1968) 238.
- [36] K. Maki, Critical fluctuation of the order parameter in a superconductor. I, *Progress of Theoretical Physics* 40 (2) (1968) 193–200.
- [37] R. S. Thompson, Microwave, flux flow, and fluctuation resistance of dirty type-II superconductors, *Physical Review B* 1 (1) (1970) 327.
- [38] J. I. Kapusta, C. Gale, Finite-temperature field theory: Principles and applications, Cambridge Monographs on Mathematical Physics, Cambridge University Press, 2011. [doi:10.1017/CB09780511535130](#).
- [39] M. L. Bellac, Thermal Field Theory, Cambridge Monographs on Mathematical Physics, Cambridge University Press, 2011. [doi:10.1017/CB09780511721700](#).
- [40] Y. Nara, A. Ohnishi, JAM mean-field update: mean-field effects on collective flow in high-energy heavy-ion collisions at  $\sqrt{s_{NN}} = 2 - 20$  GeV energies (9 2021). [arXiv:2109.07594](#).
- [41] R. Rapp, J. Wambach, H. van Hees, The Chiral Restoration Transition of QCD and Low Mass Dileptons, *Landolt-Bornstein* 23 (2010) 134. [arXiv:0901.3289](#), [doi:10.1007/978-3-642-01539-7\\_6](#).
- [42] M. Laine, NLO thermal dilepton rate at non-zero momentum, *JHEP* 11 (2013) 120. [arXiv:1310.0164](#), [doi:10.1007/JHEP11\(2013\)120](#).
- [43] J. Ghiglieri, G. D. Moore, Low Mass Thermal Dilepton Production at NLO in a Weakly Coupled Quark-Gluon Plasma, *JHEP* 12 (2014) 029. [arXiv:1410.4203](#), [doi:10.1007/JHEP12\(2014\)029](#).
- [44] D. Adamová, et al., A next-generation LHC heavy-ion experiment (1 2019). [arXiv:1902.01211](#).
- [45] M. Y. Barabanov, et al., Diquark correlations in hadron physics: Origin, impact and evidence, *Prog. Part. Nucl. Phys.* 116 (2021) 103835. [arXiv:2008.07630](#), [doi:10.1016/j.pnpnp.2020.103835](#).